Supporting Information for

Base-assisted aerobic C–H oxidation of alkylarenes with a murdochite-type oxide Mg_6MnO_8 nanoparticle catalyst

Eri Hayashi, Takatoshi Tamura, Takeshi Aihara, Keigo Kamata,* and Michikazu Hara*

Laboratory for Materials and Structures, Institute of Innovative Research, Tokyo Institute of Technology, Nagatsuta-cho 4259, Midori-ku, Yokohama 226-8503, Japan.
Email address: kamata.k.ac@m.titech.ac.jp,

Experimental Section

Materials. Solvents (*n*-octane (Kanto Chemical), chlorobenzene (TCI), and toluene (Kanto Chemical)) were pretreated with molecular sieves (3A) that were evacuated at 250 °C for 3 h.[S1] Reagents for catalytst synthesis and characterization ($Mn(OAc)_2·4H_2O$ (Kanto Chemical), $Mg(OAc)_2·4H_2O$ (Kanto Chemical), $Sr(OAc)_2·0.5H_2O$ (Kanto Chemical), $NaMnO_4·H_2O$ (Sigma-Aldrich), $MnSO_4·5H_2O$ (Kanto Chemical), DL-malic acid (Kanto Chemical), L-aspartic acid (Kanto Chemical), 5% HCl (Kanto Chemical), KI (Kanto Chemical), MgO (UBE Industries, LTD.), activated MnO_2 (Sigma-Aldrich), Mn_3O_4 (Sigma-Aldrich), MnO (Sigma-Aldrich), and $Na_2S_2O_3$ (1 M aqueous solution, Kanto Chemical)) and substrates and products for catalytic oxidation (TCI, Kanto Chemical, and Aldrich) were used as-received. Oxygen-$^{18}O_2$ (97 atom%) was purchased from ISOTEC. $SrMnO_3$ and Mn_2O_3 were synthesized by amino-aided method and characterized according to procedures given in the literature.[S2] High-surface-area β-MnO_2 nanoparticles was synthesized by a low-temperature crystallization of low-crystallinity layer-type Mn^{4+} precursors and characterized according to procedures given in the literature.[S3] DHA-d_4 was synthesized according to a literature procedure and recrystallized.[S4]

Instruments. X-ray diffraction (XRD) patterns were recorded on a diffractometer (MiniFlex 600, Rigaku; Cu Kα, λ = 1.5405 Å, 40 kV–15 mA) equipped with a high-speed 1-dimensional detector (D/teX Ultra, Rigaku). Diffraction data were collected in the range of 2θ = 10–80° in 0.02° steps with a scan rate of 20° min^{-1}. Fourier transform infrared (FTIR) spectra were obtained at a resolution of 4 cm^{-1} using a spectrometer (FT/IR-6100, Jasco) equipped with an extended KBr beam-splitting device and a mercury cadmium telluride (MCT) and a triglycine sulfate (TGS) detectors.

Raman spectra were recorded on a spectrometer (NRS-3200, Jasco) with excitation at 532 nm using a green laser. Inductively coupled plasma-atomic emission spectroscopy (ICP-AES) analyses were performed with a Shimadzu ICPS-8100 spectrometer.

Nitrogen adsorption-desorption isotherms were measured at −196 °C with a surface area and porosity analyzer (micromeritics TriStar II, Shimazu). Prior to measurement, the samples were heated at 150 °C for 3 h under vacuum to remove physiosorbed water. The Brunauer-Emmett-Teller (BET) surface areas were estimated over the relative pressure (P/P_0) range of 0.05–0.30. The morphology of the samples was examined using scanning electron microscopy (SEM; S-5500, Hitachi).

Transmission electron microscopy (TEM) observations were conducted using a JEOL JEM2100F microscope operated at an accelerating voltage of 200 kV. After directly mixing Cu grids with samples, the Cu grids were collected and mounted on a stage.

X-ray photoelectron spectroscopy (XPS) analysis were performed with Shimadzu ESCA-3200 spectrometer using Mg Kα radiation (1253.6 eV) at 8 kV and 30 mA. Samples were pressed into the pellet and fixed on a double-stick carbon tape. The binding energies were calibrated using the C 1s band at 284.6 eV. The spectrum was fitted and evaluated by the XPS Peak 4.1 program, whereas the background was subtracted using the Shirley function. The deconvoluted Mn 2p spectrum of Mg_6MnO_8 shows three peaks with binding energies of 641.8, 642.8, and 644.5 eV, which correspond to Mn(III), Mn(IV), and the shakeup peak, respectively.[S5,S6] The deconvoluted O 1s spectrum of Mg_6MnO_8 shows three peaks with binding energies of 529.2, 531.2, and 533.0 eV, which correspond to lattice oxygen, adsorbed oxygen, and adsorbed molecular water, respectively.[S5,S7]

The average oxidation states of Mn species were determined by iodometric titration using an auto titrator (Mettler Toledo, Easy Pro Titrator System). Mg_6MnO_8 samples (ca. 20 mg) was added to a mixed solution of 0.5 M HCl aq. (12 mL) and 2 M KI aq. (5 mL), and the resulting solution was titrated with an aqueous solution of 0.01 M $Na_2S_3O_3$.[S8]

Thermo gravimetry-differential thermal analysis (TG-DTA) measurement was performed with a differential thermal analyzer (Shimadzu DTG-60 differential thermal analyzer). TGA-DTA analysis was carried out at a heating rate of 10 °C min^{-1} from r.t. to 800 °C under air flow (200 mL min^{-1}).

Temperature-programmed desorption (TPD), H_2 temperature-programmed reduction (H_2-TPR), and CO_2 temperature-programmed desorption (CO_2-TPD) profile were measured on a BEL Japan BELCAT-A equipped with thermal conductivity (TCD)

and mass (Belmass) detectors. A 50 mg amount of sample for TPD and H_2-TPR was placed in a quartz cell and then heated at rate of 10 °C min^{-1} from 50 °C to 800 °C under He flow (30 mL min^{-1}) or at rate of 10 °C min^{-1} from 50 °C to 600 °C under 5% H_2/Ar flow (50 mL min^{-1}), respectively. Each catalyst (50 mg) for CO_2-TPD was pretreated under a He flow at 250 ℃ for 1 h. CO_2 adsorption was carried out over 1 h with 10% CO_2/He at 100 ℃ followed by purging with He for 30 min. The temperature was linearly increased from 100–250 ℃ (10 ℃ min^{-1}).

Liquid-phase catalytic oxidation was performed with an organic synthesizer (ALHB-80&DTC-200HZ-3000, Techno Applications), a liquid phase organic synthesizer (CHEMIST PLAZACP-1000, Sibata), or a block bath shaker (MyBL-100CS, AS ONE). The isolation of products was performed with a single channel automated flash chromatography system (Smart Flash EPCLC AI-580S, Yamazen). Gas chromatography (GC) analyses were performed on a Shimadzu GC-2025 equipped with a stabilwax capillary column (internal diameter = 0.25 mm, length = 30 m) or GC-2014 equipped with an InertCap 17 capillary column (internal diameter = 0.25 mm, length = 30 m) and a flame ionization detector. Mass spectra were recorded on a spectrometer (GCMS-QP2010 SE, Shimadzu) equipped with an InertCap 17MS capillary column (internal diameter = 0.25 mm, length = 30 m) at an ionization voltage of 70 eV.

Synthesis of murdochite-type oxide Mg_6MnO_8 nanoparticles (Mg_6MnO_8-MA) by sol-gel method using malic acid. A low-density amorphous precursor (i.e., an amorphous malate salt with the metal cations linked by carboxylate anions) decomposes starting from 400 ºC and the formation of the ramified aggregate of crystalline nanoparticles is observed at an appropriate calcination temperature.[S2a] In our previous investigation on the sol-gel methods for the synthesis of $SrMnO_3$ nanoparticles using various carboxylic acids, we found that malic acid and/or aspartic acid were more effective than typical citric acid and that the formation of an amorphous precursor by using dicarboxylic acid such as malic acid and aspartic acid with a low carbon content would be important in the present synthesis method. We separately confirmed the formation of similar Mg_6MnO_8 nanoparticles using aspartic acid instead of malic acid. Mg_6MnO_8-MA was synthesized as follows: $Mg(OAc)_2{\cdot}4H_2O$ (9.01 g, 42.0 mmol), $Mn(OAc)_2{\cdot}4H_2O$ (6.44 g, 7.0 mmol), and DL-malic acid (10.48 g, 73.5 mmol) were dissolved in water (200 mL). The pale pink solution was evaporated to dryness at 70 °C. The resulting white powder was dried at 190 °C for 1 h to give a pale-yellow powder, which is referred to as the precursor. This precursor was calcined at 550 °C for 5 h to give an analytically pure Mg_6MnO_8-MA. Yield: 2.23 g (97%). Elemental analysis:

calcd (%) for Mg_6MnO_8: Mg 44.4, Mn 16.7; found: Mg 38.0, Mn 14.7.

Procedure for oxidation with O_2 as the sole oxidant catalyzed by Mg_6MnO_8-MA. The catalytic oxidation of alkylarenes was conducted in a 20 mL Schlenk-type glass tube containing a magnetic stir bar. Typical procedures are as follows: Mg_6MnO_8-MA (0.1 g) was evacuated at 200 °C for 1 h in a Schlenk tube flowed by cooling down to room temperature. Then, **1a** (0.5 mmol), *n*-octane (2 mL), and an internal standard (naphthalene) were charged into the Schlenk tube under Ar atmosphere. After the replacement of Ar gas with O_2 gas (1 atm), the reaction solution was heated at 50 °C and periodically analyzed using GC. The products are known and were identified by comparison of their GC retention times, MS spectrum, and ^1H and ^{13}C NMR signals with the literature data. After the reaction was completed, the catalyst was recovered by filtration. The recovered Mg_6MnO_8 was washed with *n*-octane and then calcined at 400 °C for 1.5 h before recycling. In some cases, the products were isolated using a flash chromatography separation system with a silica gel column.

A larger-scale (10 mmol scale) production of 2a. The larger-scale catalytic oxidation of **1a** into **2a** was conducted in a 200 mL Schlenk-type glass tube containing a magnetic stir bar. Mg_6MnO_8-MA (0.5 g) was evacuated at 200 °C for 3 h in a Schlenk tube flowed by cooling down to room temperature. Then, **1a** (10 mmol) and *n*-octane (40 mL) were charged into the Schlenk tube under Ar atmosphere. After the replacement of Ar gas with O_2 gas (1 atm), the reaction solution was heated and stirred at 70 °C for 10 h to give **2a** in 88% GC yield. After cooling the reactor at room temperature, catalyst was removed by filtration, and then solvents were removed by evaporation. The analytically pure **2a** (1.49 g (83% yield), ≥99% purity by ^1H NMR) was isolated using a flash chromatography separation system with a silica gel column (AcOEt:hexane = 0:10 to 10:0 eluents). The amounts of surface Mn species of $MgMnO_8$-MA were estimated to be 490 μmol g^{-1} based on the BET surface area (104 m^2 g^{-1}) assuming that the (100) plane is a possible surface structure. The TOF value of $MgMnO_8$-MA was estimated to be 54 h^{-1} under the reaction conditions of eq 1.

Procedure for competitive oxidation of 1a and 9-fluorenol with O_2 as the sole oxidant catalyzed by Mg_6MnO_8-MA. The competitive oxidation of **1a** and 9-fluorenol was conducted in a 20 mL Schlenk-type glass tube containing a magnetic stir bar. The procedures are as follows: Mg_6MnO_8-MA (0.1 g) was evacuated at 200 °C for 1 h in a Schlenk tube flowed by cooling down to room temperature. Then, **1a** (0.25 mmol), 9-

fluorenol (0.25 mmol), chlorobenzene (5 mL), and an internal standard (naphthalene) were charged into the Schlenk tube under Ar atmosphere. After the replacement of Ar gas with O_2 gas (1 atm), the reaction solution was heated at 50 °C and periodically analyzed using GC. The reaction rates for the oxidation of 9-fluorenol to **2a** and **1a** to **2a** were 3.39 and 1.78×10^{-1} mM min^{-1}, respectively.

^{18}O-Labeling Experiments. The oxidation of **1a** with $^{18}O_2$ was carried out according to the literature procedures.[S2] Before the reaction, the catalyst was evacuated at 200 °C for 1 h and *n*-octane was degassed by freeze-pump-thaw cycling. The ^{18}O-Labeling experiment was carried out in a schlenk tube containing a magnetic stir bar. Catalyst (0.1 g), **1a** (0.5 mmol), *n*-octane (2 mL), and an internal standard (naphthalene) were charged into the schlenk tube under Ar atmosphere, followed by the evacuation and the introduction of 97% $^{18}O_2$ (1 atm). The reaction solution was heated at 50 °C and periodically analyzed using GC and GC-MS. The ^{18}O content in **2a** was determined by using the ratio of the peak intensity at m/z = 182 to the sum of the peak intensities at m/z = 180 and 182.

Procedure for IR measurements. The basicity on Mg_6MnO_8-MA, $SrMnO_3$, and β-MnO_2 catalysts were estimated from FT-IR measurements for chloroform-adsorbed samples at 25 °C.[S9] Samples were pressed into self-supporting disks (10 mm diameter, 7 mg and 7.8 mg for Mg_6MnO_8-MA and $SrMnO_3$, respectively; 20 mm diameter, 21 mg for β-MnO_2) and placed in an IR cell attached to a closed glass-circulation system. Prior to chloroform adsorption, the sample was dehydrated by heating at 200 °C for 1 h under vacuum. A dehydrated sample was exposed to chloroform vapor, and Figure 5c shows IR spectra for Mg_6MnO_8-MA, $SrMnO_3$, and β-MnO_2 at gas-phase chloroform pressures of 1.1×10^{-1}, 1.1×10^{-1}, and 1.2×10^{-1} kPa, respectively.

Data of products

9-Fluorenone (2a): ^{1}H NMR (400 MHz, $CDCl_3$, TMS): δ = 7.58–7.55 (m, 2H), 7.40–7.35 (m, 4H), 7.23–7.17 (m, 2H). $^{13}C\{^1H\}$ NMR (100 MHz, $CDCl_3$, TMS): δ = 193.7, 144.3, 134.6, 134.0, 128.9, 124.1, 120.2. MS (EI): *m/z* (%): 181 (15), 180 (*[M]*+, 100), 153 (6), 152 (44), 151 (21), 150 (13), 126 (7), 76 (15), 75 (6), 63 (7).

2-Fluoro-9-fluorenone (2b)[S10]: ^{1}H NMR (400 MHz, $CDCl_3$, TMS): δ = δ 7.64 (d, *J* = 7.3 Hz, 1H), 7.50–7.45 (m, 3H), 7.33 (dd, *J* = 7.6 Hz, *J* = 2.3 Hz, 1H), 7.29–7.26 (m, 1H), 7.15 (td, *J* = 8.5 Hz, *J* = 2.4 Hz, 1H); ^{13}C{^{1}H} ($CDCl_3$, 100MHz, TMS): δ = 192.6, 163.8 (d, *J* = 248.3 Hz), 144.1, 140.3, 136.5 (d, *J* = 7.2 Hz), 135.2, 134.5, 128.9, 124.8, 121.7 (d, *J* = 7.9 Hz), 121.0 (d, *J* = 23.1 Hz), 120.2, 112.1 (d, *J* = 23.5 Hz); ^{19}F{^{1}H} ($CDCl_3$, 376.4 MHz): δ = −112.7. MS (EI): *m/z* (%): 199 (*[M+1]*$^{+}$, 15), 198 (*[M]*$^{+}$, 100), 171 (5), 170 (41), 169 (15), 168 (9), 150 (6), 144 (7), 99 (7), 85 (21), 75 (5), 72 (6)

2-Bromo-9-fluorenone (2c)[S10]: ^{1}H NMR (400 MHz, $CDCl_3$, TMS): δ = 7.75 (d, *J* = 1.3 Hz, 1H), 7.65 (d, *J* = 7.4 Hz, 1H), 7.60 (dd, *J* = 7.9 Hz, *J* = 1.7 Hz, 1H), 7.52–7.47 (m, 2H), 7.38 (d, *J* = 7.9 Hz, 1H), 7.34–7.28 (m, 1H); ^{13}C{^{1}H} ($CDCl_3$, 100 MHz, TMS): δ = 192.4, 143.9, 143.2, 137.2, 136.0, 135.2, 133.9, 129.6, 127.7, 124.8, 123.1, 121.8, 120.6. MS (EI): *m/z* (%): 261 (*[M+2]*$^{+}$, 14), 260 (*[M+1]*$^{+}$,95), 259 (*[M]*$^{+}$, 15), 258 (*[M−1]*$^{+}$, 100), 232 (5), 230 (6), 179 (7), 152 (12), 151 (93), 150 (49), 149 (5), 125 (8), 116 (11), 115 (11), 99 (7), 98 (7), 90 (7), 77 (5), 76 (9), 75 (42), 74 (10), 62 (9).

2,7-Dibromo-9-fluorenone (2d)[S11]: ^{1}H NMR (400 MHz, $CDCl_3$, TMS): δ = 7.77 (d, *J* = 1.2 Hz, 2H), 7.62 (dd, *J* = 7.9 Hz, 1.6 Hz, 2H), 7.38 (d, *J* = 7.9 Hz, 2H); ^{13}C{1H} ($CDCl_3$, 100 MHz, TMS): δ = 191.0, 142.5, 137.6, 135.5, 128.0, 123.5, 122.0. MS (EI): *m/z* (%): 341 (*[M+3]*$^{+}$, 7), 340 (*[M+2]*$^{+}$, 49), 339 (*[M+1]*$^{+}$, 15), 338 (*[M]*$^{+}$, 100), 337 (*[M−1]*$^{+}$, 8), 336 (*[M−2]*$^{+}$, 52), 231 (23), 229 (24), 169 (5), 155 (8), 150 (75), 151 (10), 149 (10), 124 (5), 123 (6), 115 (10), 114 (10), 100 (5), 99 (8), 98 (10), 76 (6), 75 (44), 74 (18), 62 (10).

11-*H*-Benzo[*a*]fluoren-11-one (2e)[S12]: ^{1}H NMR (400 MHz, $CDCl_3$, TMS): δ = 8.93 (d, J=8.5Hz, 1H), 7.95 (d, *J* = 8.2Hz, 1H), 7.75 (d, *J*=8.3Hz, 1H), 7.62–7.54 (m, 3H), 7.46–7.39 (m, 3H), 7.24 (t, *J*=7.2Hz, 1H); ^{13}C{^{1}H} ($CDCl_3$, 100 MHz, TMS): δ = 195.4, 146.3, 144.0, 136.0, 134.8, 134.6, 134.3, 130.3, 129.5, 129.4, 128.6, 127.0, 126.5, 124.5, 123.9, 120.1, 118.2. MS (EI): *m/z* (%): 231 (*[M+1]*$^{+}$, 19), 230 (*[M]*$^{+}$, 100), 202 (23), 201 (13), 200 (19), 115 (7), 100 (16), 101 (24), 88 (14), 87 (6).

Xanthone (2f): ^{1}H NMR (400 MHz, $CDCl_3$, TMS): δ = 8.34 (dd, *J* = 7.6 and 1.6 Hz, 2H), 7.74–7.70 (m, 2H), 7.50–7.48 (m, 2H), 7.39–7.35 (m, 2H); ^{13}C{^{1}H} NMR (100 MHz, $CDCl_3$, TMS): δ = 177.5, 156.5, 135.1, 127.1, 124.2, 122.2, 118.3. MS (EI): *m/z* (%): 197 (14), 196 (*[M]*$^{+}$, 100), 169 (6), 168 (47), 140 (9), 139 (46), 84 (9), 69 (6), 63 (8).

Thioxanthone (2g)[S13]: ^{1}H NMR (400 MHz, $CDCl_3$, TMS): δ = 8.62 (d, *J* = 8.0 Hz, 2H), 7.63–7.56 (m, 4H), 7.48 (td, *J* = 7.4 Hz, *J* = 1.0 Hz, 2H); $^{13}C\{^{1}H\}$ NMR (100 MHz, $CDCl_3$, TMS): δ = 180.1, 137.4, 132.4, 130.0 129.5, 126.3 (d, *J* = 32). MS (EI): *m/z* (%): 214 (*[M+2]*$^{+}$, 6), 213 (*[M+1]*$^{+}$, 15), 212 (*[M]*$^{+}$, 100), 185 (8), 184 (60), 183 (8), 152 (16), 139 (26), 108 (7), 106 (6), 92 (18), 91 (7), 82 (5), 79 (14), 69 (10), 63 (5).

Anthraquinone (2h): ^{1}H NMR (400 MHz, $CDCl_3$, TMS): δ = 8.34–8.30 (m, 4H), 7.83–7.79 (m, 44H); $^{13}C\{1H\}$ NMR (100 MHz, $CDCl_3$, TMS): δ = 183.3, 134.3, 133.7, 127.4. MS (EI): *m/z* (%): 209 (*[M+1]*$^{+}$, 15), 208 (*[M]*$^{+}$, 100), 207 (*[M−1]*$^{+}$, 15), 181 (12), 180 (80), 179 (6), 153 (9), 152 (74), 151 (37), 150 (19), 126 (11), 90 (9), 77 (9), 76 (53), 75 (19), 74 (10), 63 (14), 51 (5), 50 (16),

Dibenzosuberone (2i)[S14]: ^{1}H NMR (400 MHz, $CDCl_3$, TMS): δ = 8.01 (d, *J* = 7.8 Hz, 2H), 7.42 (t, *J* = 7.4 Hz, 2H), 7.33 (t, *J* = 7.4 Hz, 2H), 7.22 (d, *J* = 7.5 Hz, 2H), 3.21 (s, 4H); $^{13}C\{^{1}H\}$ NMR (100 MHz, $CDCl_3$, TMS): δ = 195.7, 142.1, 138.8, 132.5, 130.7, 129.4, 126.8, 35.1. MS (EI): *m/z* (%): 209 (*[M+1]*$^{+}$, 16), 208 (*[M]*$^{+}$, 100), 207 (*[M−1]*$^{+}$, 38), 193 (10), 181 (9), 180 (57), 179 (65), 178 (53), 177 (9), 176 (13), 166 (6), 165 (39), 152 (19), 151 (9), 115 (5), 103 (8), 102 (5), 90 (13), 89 (44), 88 (10), 83 (5), 77 (12) 76 (24), 75 (6), 63 (12), 51 (8), 39 (6).

Benzophenone (2j): ^{1}H NMR (400 MHz, $CDCl_3$, TMS): δ = 7.82–7.79 (m, 4H), 7.61−7.57 (m, 2H), 7.51–7.46 (m, 4H). $^{13}C\{^{1}H\}$ NMR (100 MHz, $CDCl_3$, TMS): δ = 197.0, 138.0, 132.7, 130.4, 128.6. MS (EI): *m/z* (%): 183 (7), 182 (*[M]*+, 47), 181 (*[M−1]*$^{+}$, 8), 106 (8), 105 (100), 78 (18), 77 (56), 76 (5), 51(18), 50 (7).

2-Benzoylpyridine (2k)[S15]: ^{1}H NMR (400 MHz, $CDCl_3$, TMS): δ = 8.72 (d, *J* = 4.6 Hz, 1H), 8.08–8.03 (m, 3H), 7.90 (t, *J* = 7.7 Hz, 1H), 7.59 (t, *J* = 7.4 Hz, 1H), 7.50–7.46 (m, 3H); $^{13}C\{^{1}H\}$ NMR (100 MHz, $CDCl_3$, TMS): δ = 193.9, 155.4, 148.7, 137.1, 136.5, 133.0, 131.1, 128.3, 126.2, 124.7. MS (EI): *m/z* (%): 183 (*[M]*$^{+}$, 18), 182 (*[M−1]*$^{+}$, 42), 156 (10), 155 (83), 154 (28), 127 (7), 106 (7), 105 (86), 78 (17), 77 (100), 76 (6), 52 (7), 51 (39), 50 (10).

3-Benzoylpyridine (2l)[S16]: ^{1}H NMR (400 MHz, $CDCl_3$, TMS): δ = 9.00 (s, 1H), 8.82 (d, *J* = 4.8 Hz, 1H), 8.12 (d, *J* = 7.8 Hz, 1H), 7.82 (d, *J* = 7.8 Hz, 2H), 7.64 (t, *J* = 7.3 Hz, 1H), 7.52 (t, *J* = 7.6 Hz, 2H), 7.45 (dd, *J* = 7.5, 4.9 Hz, 1H); $^{13}C\{^{1}H\}$ NMR (100 MHz, $CDCl_3$, TMS): δ = 195.0, 153.0, 151.1, 137.3, 137.0, 133.4, 133.3, 130.1 128.8, 123.5.

MS (EI): *m/z* (%): 184 (*[M+1]*$^+$, 10), 183 (*[M]*$^+$, 73), 182 (*[M−1]*$^+$, 28), 154 (6), 106 (26), 105 (100), 78 (33), 77 (73), 51 (37), 50 (10).

4-Benzoylpyridine (2m)[S17]: ^{1}H NMR (400 MHz, $CDCl_3$, TMS): δ = 8.81 (d, *J* = 5.8 Hz, 2H), 7.82 (d, *J* = 7.3 Hz, 2H), 7.65 (t, *J* = 7.4 Hz, 1H), 7.58 (d, *J* = 5.8 Hz, 2H), 7.52 (t, *J* = 7.6 Hz, 2H); ^{13}C{^{1}H} NMR (100 MHz, $CDCl_3$, TMS): δ = 195.2, 150.5, 144.6, 136.1, 133.6, 130.3, 128.8, 123.0. MS (EI): *m/z* (%): 184 (*[M+1]*$^+$, 5), 183 (*[M]*$^+$, 35), 106 (13), 105 (100), 78 (14), 77 (63), 51 (29), 50 (7).

Benzil (2n): ^{1}H NMR (400 MHz, $CDCl_3$, TMS): δ = 7.98 (d, *J* = 7.8 Hz, 4H), 7.66 (t, *J* = 7.4 Hz, 2H), 7.51 (t, *J* = 7.7 Hz, 4H); ^{13}C{^{1}H} NMR (100 MHz, $CDCl_3$, TMS): δ = 194.7, 135.0, 133.3, 130.0, 129.2. MS (EI): *m/z* (%): 211 (*[M+1]*$^+$, 0.4), 106 (11), 105 (100), 77 (60), 51 (19).

Indole (2o): ^{1}H NMR (400 MHz, $CDCl_3$, TMS): δ = 8.08 (br, 1H), 7.64 (d, *J* = 7.8, 1H), 7.38 (d, *J* = 8.1 Hz, 1H), 7.21–7.10 (m, 3H), 6.55 (s, 1H); ^{13}C{^{1}H} NMR (100 MHz, $CDCl_3$, TMS): δ = 136.0, 128.1, 124.2, 122.2, 120.9, 120.0, 111.1, 102.8. MS (EI): *m/z* (%): 117 (*[M]*$^+$, 100), 90 (46), 89 (32), 59 (12), 63 (11), 118 (10), 116 (8), 39 (5).

Phthalide (2p)[S13]: ^{1}H NMR (400 MHz, $CDCl_3$, TMS): δ = 7.93 (d, *J* = 7.7 Hz, 1H), 7.69 (t, *J* = 7.5 Hz, 1H), 7.56–7.49 (m, 2H), 5.33 (s, 2H); ^{13}C{^{1}H} NMR (100 MHz, $CDCl_3$, TMS): δ = 171.1, 146.7, 134.1, 129.2, 126.0, 122.2, 69.7. MS (EI): *m/z* (%): 134 (*[M]*$^+$, 32), 133 (*[M−1]*$^+$, 12), 106 (8), 105 (100), 77 (44), 76 (10), 51 (15), 50 (12).

References

(S1) Williams, D. B.; Lawton, M. Drying of Organic Solvents: Quantitative Evaluation of the Efficiency of Several Desiccants. *J. Org. Chem.* **2010**, *75*, 8351–8354.

(S2) (*a*) Sugahara, K.; Kamata, K.; Muratsugu, S.; Hara, M. Amino Acid-Aided Synthesis of a Hexagonal $SrMnO_3$ Nanoperovskite Catalyst for Aerobic Oxidation. *ACS Omega* **2017**, *2*, 1608–1616. (*b*) Kamata, K.; Sugahara, K.; Kato, Y.; Muratsugu, S.; Kumagai, Y.; Oba, F.; Hara, M. Heterogeneously Catalyzed Aerobic Oxidation of Sulfides with a $BaRuO_3$ Nanoperovskite. *ACS Appl. Mater. Interfaces* **2018**, *10*, 23792–23801. (*c*) Shibata, S.; Sugahara, K.; Kamata, K.; Hara, M. Liquid-Phase Oxidation of Alkanes with Molecular Oxygen Catalyzed by High Valent Iron-Based Perovskite. *Chem. Commun.* **2018**, *54*, 6772–6775. (*d*) Sugawara, Y.; Kamata, K.; Yamaguchi, T. Extremely Active Hydrogen Evolution

Catalyst Electrochemically Generated from a Ruthenium-Based Perovskite-Type Precursor. *ACS Appl. Energy Mater.* **2019**, *2*, 956–960. (*e*) Shibata, S.; Kamata, K.; Hara, M. Aerobic Oxidative C=C Bond Cleavage of Aromatic Alkenes by a High Valency Iron-Containing Perovskite Catalyst. *Catal. Sci. Technol.* **2021**, *11*, 2369–2373. (*f*) Sugawara, Y.; Hihara, T.; Anilkumar, G. M.; Kamata, K.; Yamaguchi, T. Metal Oxide Electrocatalyst Support for Carbon-Free Durable Electrodes with Excellent Corrosion Resistance at High Potential Conditions. *Sustain. Energy Fuels* **2021**, *5*, 1374–1378. (*g*) Sugawara, Y.; Kamata, K.; Ishikawa, A.; Tateyama, Y.; Yamaguchi, T. Efficient Oxygen Evolution Electrocatalysis on $CaFe_2O_4$ and its Reaction Mechanism. *ACS Appl. Energy Mater.* **2021**, *4*, 3057–3066.

(S3) (*a*) Hayashi, E.; Yamaguchi, Y.; Kamata, K.; Tsunoda, N.; Kumagai, Y.; Oba, F.; Hara, M. Effect of MnO_2 Crystal Structure on Aerobic Oxidation of 5-Hydroxymethylfurfural to 2,5-Furandicarboxylic Acid. *J. Am. Chem. Soc.* **2019**, *141*, 890–900. (*b*) Yamaguchi, Y.; Aono, R.; Hayashi, E.; Kamata, K.; Hara, M. Template-Free Synthesis of Mesoporous β-MnO_2 Nanoparticles Structure, Formation Mechanism, and Catalytic Properties. *ACS Appl. Mater. Interfaces* **2020**, *12*, 36004–36013. (*c*) Hayashi, E.; Yamaguchi, Y.; Kita, Y.; Kamata, K.; Hara, M. One-Pot Aerobic Oxidative Sulfonamidation of Aromatic Thiols with Ammonia by a Dual-Functional β-MnO_2 Nanocatalyst. *Chem. Commun.* **2020**, *56*, 2095–2098.

(S4) Goldsmith, C. R.; Jonas, R. T.; Stack, T. D. P. C−H Bond Activation by a Ferric Methoxide Complex: Modeling the Rate-Determining Step in the Mechanism of Lipoxygenase. *J. Am. Chem. Soc.* **2002**, *124*, 83–96.

(S5) Tang, Q.; Jiang, L.; Liu, J.; Wang, S.; Sun, G. Effect of Surface Manganese Valence of Manganese Oxides on the Activity of the Oxygen Reduction Reaction in Alkaline Media. *ACS Catal.* **2014**, *4*, 457–463.

(S6) Nesbitt, H. W.; Banerjee, D. Interpretation of XPS Mn(2p) Spectra of Mn Oxyhydroxides and Constraints on the Mechanism of MnO_2 Precipitation. *Am. Mineral.* **1998**, *83*, 305–315.

(S7) Kang, M.; Park, E. D.; Kim, J. M.; Yie, J. E. Manganese Oxide Catalysts for NO_x Reduction with NH_3 at Low Temperatures. *Appl. Catal. A: Gen.* **2007**, *327*, 261–269.

(S8) Rormark, L.; Wiik, K.; Stolen, S.; Grande, T. Oxygen Stoichiometry and Structural Properties of $La_{1-x}A_xMnO_{3\pm\delta}$ (A = Ca or Sr and $0 \leq x \leq 1$). *J. Mater. Chem.* **2002**, *12*, 1058–1067.

(S9) (*a*) Tamura, M.; Shimizu, K.; Satsuma, A. Comprehensive IR Study on Acid/Base

Properties of Metal Oxides. *Appl. Catal. A: Gen*. **2012**, *433–434*, 135–145. (*b*) Komanoya, T.; Nakajima, K.; Kitano, M.; Hara, M. Synergistic Catalysis by Lewis Acid and Base Sites on ZrO_2 for Meerwein–Ponndorf–Verley Reduction. *J. Phys. Chem. C*. **2015**, *119*, 26540–26546.

(S10) Wertz, S.; Leifert, D.; Studer, A. Cross Dehydrogenative Coupling via Base-Promoted Homolytic Aromatic Substitution (BHAS): Synthesis of Fluorenones and Xanthones. *Org. Lett.* **2013**, *15*, 928–931.

(S11) Zhang, X.; Ji, X.; Jiang, S.; Liu, L.; Weeks, B. L.; Zhang, Z. Highly Efficient Synthesis of 9-Fluorenones from 9H-Fluorenes by Air Oxidation. *Green Chem.* **2011**, *13*, 1891–1896.

(S12) Zhao, Y.-B.; Mariampillai, B.; Candito, D. A.; Laleu, B.; Li, M.; Lautens, M. *Angew. Chem., Int. Ed.* Exploiting the Divergent Reactivity of Aryl–Palladium Intermediates for the Rapid Assembly of Fluorene and Phenanthrene Derivatives. **2009**, *48*, 1849–1852.

(S13) Geng, P.; Tang, Y.; Pan, G.; Wang, W.; Hu, J.; Cai, Y. A g-C_3N_4-Based Heterogeneous Photocatalyst for Visible Light Mediated Aerobic Benzylic C–H Oxygenations. *Green Chem.* **2019**, *21*, 6116–6122.

(S14) Ye, D.; Liu, Z.; Sessler, J. L.; Lei, C. Base-Free Oxidation of Alcohols Enabled by Nickel(ii)-Catalyzed Transfer Dehydrogenation. *Chem. Commun.* **2020**, *56*, 11811–11814.

(S15) Joshi, A.; Semwal, R.; Suresh, E.; Adimurthy, S. Pd-Catalyzed Regioselective Synthesis of 2,6-Disubstituted Pyridines through Denitrogenation of Pyridotriazoles and 3,8-Diarylation of Imidazo[1,2-a]pyridines. *Chem. Commun.* **2019**, *55*, 10888–10891.

(S16) Wang, H.; Liu, J.: Qu, J.-P.; Kang, Y.-B. Overcoming Electron-Withdrawing and Product-Inhibition Effects by Organocatalytic Aerobic Oxidation of Alkylpyridines and Related Alkylheteroarenes to Ketones. *J. Org. Chem.* **2020**, *85*, 3942–3948.

(S17) Zhu, D.-L.; Wu, Q.; Young, D. J.; Wang, H.; Ren, Z.-G.; Li, H.-X. Acyl Radicals from *α*-Keto Acids Using a Carbonyl Photocatalyst: Photoredox-Catalyzed Synthesis of Ketones. *Org. Lett.* **2020**, *22*, 6832−6837.

(S18) Kawasaki, S.; Kamata, K.; Hara, M. Dioxygen Activation by a Hexagonal $SrMnO_3$ Perovskite Catalyst for Aerobic Liquid-Phase Oxidation. *ChemCatChem* **2016**, *8*, 3247–3253.

(S19) Shaabani, A.; Hezarkhani, Z.; Badali, E. Cellulose Supported Manganese Dioxide Nanosheet Catalyzed Aerobic Oxidation of Organic Compounds. *RSC Adv.* **2015**,

5, 61759–61767.

(S20) Shaabani, A.; Boroujeni, M. B.; Laeini, M. S. Porous Chitosan–MnO_2 Nanohybrid: a Green and Biodegradable Heterogeneous Catalyst for Aerobic Oxidation of Alkylarenes and Alcohols. *Appl. Organomet. Chem.* **2016**, *30*, 154–159.

(S21) Uematsu, T.; Miyamoto, Y.; Ogasawara, Y.; Suzuki, K.; Yamaguchi, K.; Mizuno, N. Molybdenum-Doped α-MnO_2 as an Efficient Reusable Heterogeneous Catalyst for Aerobic Sulfide Oxygenation. *Catal. Sci. Technol.* **2016**, *6*, 222–233.

(S22) Nakai, S.; Uematsu, T.; Ogasawara, Y.; Suzuki, K.; Yamaguchi, K.; Mizuno, N. Aerobic Oxygenation of Alkylarenes over Ultrafine Transition-Metal-Containing Manganese-Based Oxides. *ChemCatChem* **2018**, *10*, 1096–1106.

(S23) Zhang, P.; Lu, H.; Zhou, Y.; Zhang, L.; Wu, Z.; Yang, S.; Shi, H.; Zhu, Q.; Chen, Y.; Dai, S. Mesoporous $MnCeO_x$ Solid Solutions for Low Temperature and Selective Oxidation of Hydrocarbons. *Nat. Commun.* **2015**, *6*, 8446.

(S24) Kuwahara, Y.; Yoshimura, Y.; Yamashita, H. Liquid-Phase Oxidation of Alkylaromatics to Aromatic Ketones with Molecular Oxygen over a Mn-Based Metal–Organic Framework. *Dalton Trans.* **2017**, *46*, 8415–8421.

(S25) Wang, A.; Zhou, W.; Sun, Z.; Zhang, Z.; Zhang, Z.; He, M.; Chen, Q. Mn(III) Active Site in Hydrotalcite Efficiently Catalyzes the Oxidation of Alkylarenes with Molecular Oxygen. *Mol. Catal.* **2021**, *499*, 111276.

(S26) Opembe, N. N.; Son, Y.-C.; Sriskandakumar, T.; Suib, S. L. Kinetics and Mechanism of 9H-Fluorene Oxidation Catalyzed by Manganese Oxide Octahedral Molecular Sieves. *ChemSusChem* **2008**, *1*, 182–185.

(S27) Sahin, Y.; Sika-Nartey, A. T.; Ercan, K. E.; Kocak, Y.; Senol, S.; Ozensoy, E.; Türkmen, Y. E. Precious Metal-Free $LaMnO_3$ Perovskite Catalyst with an Optimized Nanostructure for Aerobic C−H Bond Activation Reactions: Alkylarene Oxidation and Naphthol Dimerization. *ACS Appl. Mater. Interfaces* **2021**, *13*, 5099−5110.

(S28) Zhou, L.; Lu, T.; Xu, J.; Chen, M.; Zhang, C.; Chen, C.; Yang, X.; Xu, J. Synthesis of Hierarchical MeAPO-5 Molecular Sieves–Catalysts for the Oxidation of Hydrocarbons with Efficient Mass Transport. *Microporous Mesoporous Mater.* **2012**, *161*, 76–83.

(S29) Mahyari, M.; Laeini, M. S.; Shaabani, A. Aqueous Aerobic Oxidation of Alkyl Arenes and Alcohols Catalyzed by Copper(II) Phthalocyanine Supported on Three-Dimensional Nitrogen-Doped Graphene at Room Temperature. *Chem. Commun.* **2014**, *50*, 7855–7857.

(S30) Luo, J.; Wang, Y.; Wang, F.; Li, F.; Li, L.; Zhao, N.; Xiao, F. Aerobic Oxidation of

Fluorene to Fluorenone over Copper-Doped Co_3O_4 with a High Specific Surface Area. *ACS Sustainable Chem. Eng.* **2020**, *8*, 2568−2576.

(S31) Chauhana, P.; Yan, N. Nanocrystalline Cellulose Grafted Phthalocyanine: a Heterogeneous Catalyst for Selective Aerobic Oxidation of Alcohols and Alkyl Arenes at Room Temperature in a Green Solvent. *RSC Adv.* **2015**, *5*, 37517–37520.

(S32) Nie, S.; Wang, J.; Huang, X.; Niu, X.; Zhu, L.; Yao, X. Ball-Milled Co−N−C Nanocomposite for Benzylic C−H Bond Oxidation: a Facile, Practical, and Recyclable Catalyst under Neat Conditions and Atmospheric Pressure Oxygen. *ACS Appl. Nano Mater.* **2018**, *1*, 6567−6574.

(S33) Shaabani, A.; Hezarkhani, Z.; Nejad, M. K. Cr- and Zn-Substituted Cobalt Ferrite Nanoparticles Supported on Guanidine–Modified Graphene Oxide as Efficient and Recyclable Catalysts. *J Mater. Sci.* **2017**, *52*, 96–112.

(S34) Shaabani, A.; Shaabani, S.; Afaridoun, H. Highly Selective Aerobic Oxidation of Alkyl Arenes and Alcohols: Cobalt Supported on Natural Hydroxyapatite Nanocrystals. *RSC Adv.* **2016**, *6*, 48396–48404.

(S35) Dapurkar, S. E.; Kawanami, H.; Yokoyama, T.; Ikushima, Y. Solvent-Free Selective Oxidation of Benzylic Compounds over Chromium Containing Mesoporous Molecular Sieve Catalyst at 1 atm O_2. *Catal. Commun.* **2009**, *10*, 1025–1028.

(S36) Jana, S. K.; Wub, P.; Tatsumi, T. NiAl Hydrotalcite as an Efficient and Environmentally Friendly Solid Catalyst for Solvent-Free Liquid-Phase Selective Oxidation of Ethylbenzene to Acetophenone with 1 atm of Molecular Oxygen. *J. Catal.* **2006**, *240*, 268–274.

(S37) Wang, Y.; Li, H.; Yao, J.; Wanga, X.; Antonietti, M. Synthesis of Boron Doped Polymeric Carbon Nitride Solids and Their Use as Metal-Free Catalysts for Aliphatic C–H Bond Oxidation. *Chem. Sci.* **2011**, *2*, 446–450.

(S38) Sharma, A. S.; Kaur, H. Sustainable Protocol for Benzylic-CH_2 Oxidation with Dioxygen to Phenones Using AuNPs@Resin Beads. *ChemistrySelect* **2017**, *2*, 10112–10117.

(S39) Yamaguchi, K.; Mizuno, N. Heterogeneously Catalyzed Liquid-Phase Oxidation of Alkanes and Alcohols with Molecular Oxygen. *New J. Chem.* **2002**, *26*, 972–974.

(S40) Kamata, K.; Kasai, J.; Yamaguchi, K.; Mizuno, N. Efficient Heterogeneous Oxidation of Alkylarenes with Molecular Oxygen. *Org. Lett.* **2004**, *6*, 3577–3580.

(S41) Yoshida, A.; Takahashi, Y.; Ikeda, T.; Azemoto, K.; Naito, S. Catalytic Oxidation of Aromatic Alcohols and Alkylarenes with Molecular Oxygen over Ir/TiO_2. *Catal. Today* **2011**, *164*, 332–335.

(S42) Kawabata, H.; Hayashi, M. Benzylic Oxygenation of Alkylarenes with Molecular Oxygen in the Presence of Activated Carbon. *Tetrahedron Lett.* **2004**, *45*, 5457–5459.

(S43) Tabata, K.; Karasuda, T.; Suzuki, E. N_2O Decomposition over $(Mg_{6-x}A_x)MnO_8$ (A = Li, Al). *J. Mater. Sci.* **2000**, *35*, 4031–4037.

(S44) Taguchi, H.; Ohota, A.; Nagao, M. Carbon Monoxide Oxidation on $(Mg_{6-x}Al_x)MnO_8$ ($0 \leq x \leq 0.6$). *J. Mater. Sci.* **1996**, *31*, 5697–5700.

(S45) Tamilarasan, S.; Laha, S.; Natarajan, S.; Gopalakrishnan, J. Li_2MnO_3: a Rare Red-Coloured Manganese(IV) Oxide Exhibiting Tunable Red–Yellow–Green Emission. *J. Mater. Chem. C* **2015**, *3*, 4794–4800.

(S46) Taguchi, H.; Nagao, M. Synthesis of Mg_6MnO_8 through the Sol-Gel Process. *J. Mater. Sci. Lett.* **1991**, *10*, 658–659.

(S47) Cimino, A.; Indovina, V. Activity of Mn^{3+} and Mn^{4+} Ions Dispersed in MgO for N_2O Decomposition. *J. Catal*. **1970**, *17*, 54–70.

(S48) Yusuf, S.; Neal, L. M.; Li, F. Effect of Promoters on Manganese-Containing Mixed Metal Oxides for Oxidative Dehydrogenation of Ethane via a Cyclic Redox Scheme. *ACS Catal.* **2017**, *7*, 5163−5173.

(S49) Dudek, R. B.; Gao, Y.; Zhang, J.; Lii, F. Manganese-Containing Redox Catalysts for Selective Hydrogen Combustion Under a Cyclic Redox Scheme. *AIChE J.* **2018**, *64*, 3141–3150.

(S50) Mariscal, R.; Soria, J.; Pena, M. A.; Fierro, J. L. G. Features of Li-Mn-MgO Catalysts and Their Relevance in the Oxidative Coupling of Methane. *J. Catal.* **1994**, *147*, 535–543.

(S51) Aritani, H.; Yamada, H.; Nishio, T.; Imamura, S.; Hasegawa, S.; Tanaka, T.; Yoshida, S. Formation of Defects in Near-Surface Region over Li or Mn-Doped MgO Studied by Mg K-Edge XANES. *Chem. Lett.* **1999**, *4*, 359–360.

(S52) Lee, J.; Seymour, I. D.; Pell, A. J.; Dutton, S. E.; Grey, C. P. A Systematic Study of ^{25}Mg NMR in Paramagnetic Transition Metal Oxides: Applications to Mg-Ion Battery Materials. *Phys. Chem. Chem. Phys.* **2017**, *19*, 613–625.

(S53) Dunstan, M. T.; Jain, A.; Liu, W.; Ong, S. P.; Liu, T.; Lee, J.; Persson, K. A.; Scott, S. A.; Dennisg, J. S.; Grey, C. P. Large Scale Computational Screening and Experimental Discovery of Novel Materials for High Temperature CO_2 Capture. *Energy Environ. Sci.* **2016**, *9*, 1346–1360.

(S54) Valverde-Diez, N.; Grande-Fernandez, D. Ternary Compounds of the System Mg-Mn-O as Oxygen Sensors. *Solid State Ion.* **1988**, *28–30*, 1697–700.

(S55) Kasper, J. S.; Prener, J. S. The Crystal Structure of Mg_6MnO_8. *Acta Cryst.* **1954**, *7*,

246–248.

(S56) Porta, P.; Valigi, M. Magnetic and Optical Investigation of Mg_6MnO_8. *J. Solid State Chem.* **1973**, *6*, 344–347.

(S57) Bordwell, F. G.; Bausch, M. J. Acidity-Oxidation-Potential (AOP) Values as Estimates of Relative Bond Dissociation Energies and Radical Stabilities in Dimethyl Sulfoxide Solution. *J. Am. Chem. Soc.* **1986**, *108*, 1979–1985.

(S58) Zhang, X.; Bordwell, F. G. Acidities and Homolytic Bond Dissociation Energies of the Acidic Carbon-Hydrogen Bonds in Radical Cations. *J. Org. Chem.* **1992**, *57*, 4163–4168.

(S59) Bordwell, F. G.; Cheng, J.-P.; Ji, G.-Z.; Satish, A. V.; Zhang, X. Bond Dissociation Energies in DMSO Related to the Gas Phase Values. *J. Am. Chem. Soc.* **1991**, *113*, 9790–9795.

(S60) Cheng, J.-P.; Handoo, K. L.; Parker, V. D. Hydride Affinities of Carbenium Ions in Acetonitrile and Dimethyl Sulfoxide Solution. *J. Am. Chem. Soc.* **1993**, *115*, 2655–2660.

(S61) Handoo, K. L.; Cheng, J.-P.; Parker, V. D. Hydride Affinities of Organic Radicals in Solution. A Comparison of Free Radicals and Carbenium Ions as Hydride Ion Acceptors. *J. Am. Chem. Soc.* **1993**, *115*, 5067–5072.

Table S1. Additive-free Heterogeneous Catalyst Systems for the Oxidation of Fluorene (**1a**) with O_2 as the sole oxidant

Entry	Catalyst/additive	Oxidant	Solvent	Temp. (°C)	Time (h)	Yield (%)	Reaction rate[a] (mmol g_{cat}^{-1} h^{-1})	Ref.
			Mn-based catalyst					
1	$SrMnO_3$ (aspartic acid-aided method)	O_2 (1 atm)	*n*-octane	60	24	96	0.2	S2(*a*)
2	$SrMnO_3$ (polymerize complex method)	O_2 (1 atm)	*n*-octane	80	12	93	0.4	S18
3	MnO_2@wool	air (1 atm)	*o*-xylene	reflux	9	99	1.0	S19
4	MnO_2/porous chitosan	air	*p*-xylene	100	4	95	5.9	S20
5	Mo-MnO_2	O_2 (5 atm)	*o*-dichlorobenzene	150	6	90	1.5	S21
6	Ni-MnO_x	O_2 (1 atm)	*n*-octane	80	1	99	9.9	S22
7	$Mn_{0.5}Ce_{0.5}O_x$	O_2 (10 atm)	CH_3CN	110	4	82	6.8	S23
8[d]	Mn-MOF-74	O_2 (5 mL min^{-1})	*m*-dichlorobenzene	135	9	24	19.6	S24
9[e]	Ni_2Mn-LDH	O_2 (1 atm)	dodecane	120	3.5	81	1.2	S25
10[f]	OMS-2	air (1 atm)	isooctane	reflux	4	99	5.0	S26
11	$LaMnO_3$	O_2 (1 atm)	heptane	80	24	96	0.1	S27
12[g]	MnAlPO-5-meso	O_2 (5 atm)	CH_3CN	120	5	24	1.0	S28
			metal-based catalyst					
13[g]	FeAlPO-5-meso	O_2 (5 atm)	CH_3CN	120	5	15	0.6	S28
14[h]	CuTSPc@3D-(N)GFs	air (1 atm)	H_2O	r.t.	12	96	16.0	S29
15	Cu-doped Co_3O_4	O_2 (10 atm)	cyclohexane	90	4	99	5.0	S30
16[i]	NCC-PC	air (1 atm, bubbling)	H_2O	r.t.	10	88	0.3	S31
17	Co−N−C nanocomposite	O_2 (1 atm, balloon)	DMSO	140	20	81	25.3	S32
18[j]	$CrCoFeO_4$@G–GO	air (1 atm)	*o*-xylene	reflux	4	96	2.0	S33
19[k]	Co–NHAp	air	*p*-xylene	100	8	85	0.6	S34
20[l]	CrMCM-41	O_2 (1 atm)	–	95	24	23	2.9	S35

21	$BaFeO_{3-\delta}$	O_2 (1 atm)	*n*-octane	80	96	59	0.03	S2(c)
22[m]	NiAl HT	O_2 (5 mL min^{-1})	–	135	5	58	5.8	S36
23[n]	$CNB_{0.15}$	O_2 (10 atm)	CH_3CN	130	24	45	0.4	S37
24[o]	AuNPs@resin	O_2 (1 atm)	CH_3CN	80	20	30	0.1	S38
25	Ru^{3+}-substituted silicotungstate	O_2 (1 atm)	isobutyl acetate	110	96	10	0.7	S39
26	$Ru(OH)_x/Al_2O_3$	O_2 (1 atm)	*o*-dichlorobenzene	170	4	93	0.9	S40
27	Ir/TiO_2	O_2 (1 atm)	Mesitylene	150	50	62	0.2	S41
			carbon-based catalyst					
28[p]	g-C_3N_4	O_2 (1 atm, balloon)	H_2O	r.t. + blue LED	24	62	0.3	S13
29	activated carbon (Shirasagi KL)	O_2 (?)	*m*-xylene	120	24	83	0.2	S42

[a]Reaction rate per gram (mmol h^{-1} g^{-1}) = (**2a** (mmol)) / time (h) × catalyst (g). [b]The reaction rate per gram could not be estimated because of no information about the amount of catalyst. [c]The reaction rate per gram could not be estimated because of no information about the amount of **1a**. [d]MOF = metal organic frameworks. [e]LDH = layered double hydroxide. [f]OMS-2 = Cryptomelane-type manganese oxide. [g]ALPO = aluminophosphate. [h]TSPc = tetrasulfophthalocyanine, 3D-(N)GFs = three-dimensional nitrogen-doped graphene-based frameworks. [i]NCC-PC = nanocrystalline cellulose-anionic copper tetrasulfonate phthalocyanine. [j]$CrCoFeO_4$@G–GO = Cr-substituted cobalt ferrite nanoparticles supported on guanidine-grafted graphene oxide nanosheets. [k]NHAp = natural hydroxyapatite. [l]MCM-41= Mobil crystalline material 41. [m]HT = hydrotalcite. [n]CNB = boron-doped polymeric carbon nitride. [o]NPs = nanoparticles. [p]g-C_3N_4 = graphitic carbon nitride.

Table S2. Surface area, preparation method, and regent of reported Mg_6MnO_8

Entry	Synthetic method	Reagents	Surface area ($m^2\ g^{-1}$)	Application	Ref.
1	sol-gel method (400 °C, 2 h → 700 °C, 6 h)	$Mg(OAc)_2 \cdot 4H_2O$, $Mn(OAc)_2 \cdot 4H_2O$	15	catalyst (N_2O decomposition)	S43
2	sol-gel method (400 °C, 2 h, O_2 → 700 °C, 6 h, O_2)	$Mg(OAc)_2 \cdot 4H_2O$, $Mn(OAc)_2 \cdot 4H_2O$	15	catalyst (CO oxidation)	S44
3	sol-gel method (250 °C, 2 h → 750 °C, 12 h)	$Mg(OAc)_2 \cdot 4H_2O$, $Mn(OAc)_2 \cdot 4H_2O$	–	–	S45
4	sol-gel method (500–800 °C, 6 h, O_2)	$Mg(OAc)_2 \cdot 4H_2O$, acetic acid, $Mn(OAc)_2 \cdot 4H_2O$	–	–	S46
5	impregnation method (1000 °C, ? h)	$Mn(NO_3)_2$, MgO	–	catalyst (N_2O decomposition)	S47
6	incipient wetness impregnation method (450 °C, 3 h → 900 °C, 8 h)	$Mn(NO_3)_2$, MgO	4	catalyst (oxidative dehydrogenation of ethane)	S48
7	incipient wetness impregnation method (450 °C, 3 h → 900 °C, 8 h)	$Mn(NO_3)_2$, MgO	7	catalyst (selective hydrogen combustion)	S49
8	incipient wetness impregnation method (800 °C, 4 h)	$Mn(NO_3)_2 \cdot 4H_2O$, MgO	–	catalyst (oxidative coupling of methane)	S50
9	incipient wetness impregnation method (600 °C, 3 h)	$Mn(NO_3)_2 \cdot 6H_2O$, MgOH	–	–	S51
10	solid phase method (900 °C, 12 h)	MgO, MnO_2	–	Mg-ion batteries	S52
11	solid phase method (900 °C, 12 h)	MgO, MnO_2	2	CO_2 capture	S53
12	solid phase method	MgO, MnO_2	–	oxygen sensor	S54
13	solid phase method (1100, 5 h, O_2)	$Mn(CO_3)$, MgO	–	–	S55
14	coprecipitation method (700 or 800 °C, few hours)	$Mg(OAc)_2 \cdot 4H_2O$, $Mn(OAc)_2 \cdot 4H_2O$	–	–	S56

Table S3. Comparison of surface physicochemical properties of manganese oxides

	Mg_6MnO_8-MA	$SrMnO_3$[b]	β-MnO_2[c]
Oxidation states of surface Mn species[a]	3.7	3.6	3.5
Amounts of adsorbed oxygen species (%)[a]	33	38	29
S_{BET} (m^2 g^{-1})	104	47	106

[a]Estimated by XPS analysis. [b]Data from ref. S2(*a*). [c]Data from ref. S3(*b*).

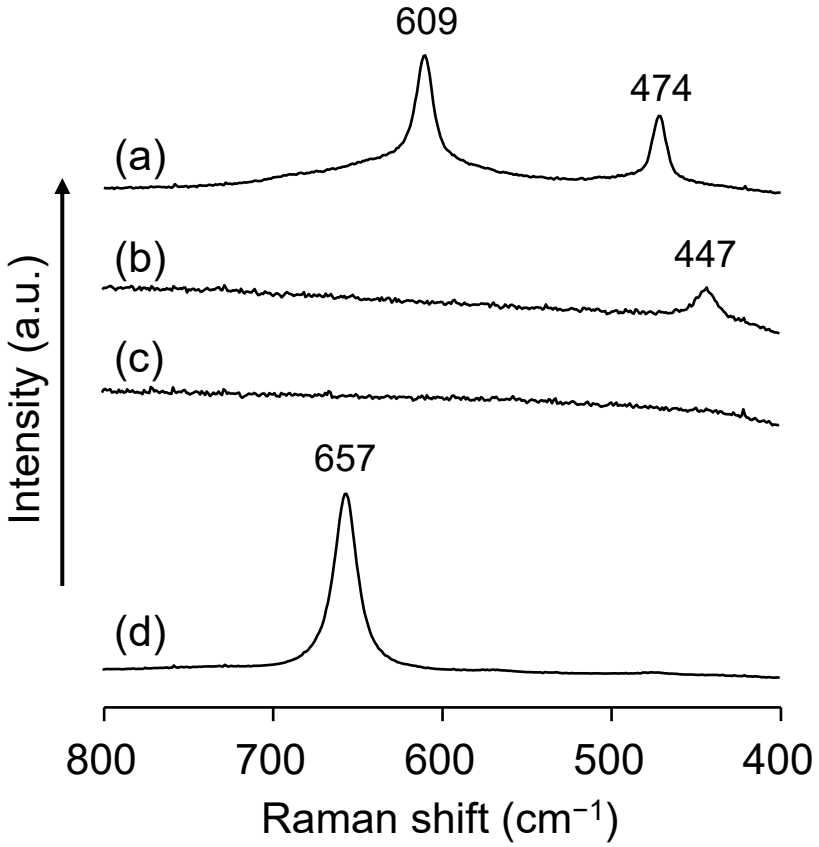

Figure S1. Raman spectra for (a) Mg_6MnO_8-MA, (b) MgO, (c) activated MnO_2 (Aldrich), and (d) Mn_2O_3.

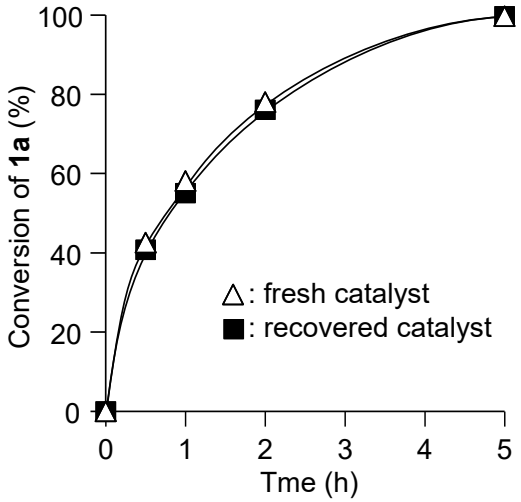

Figure S2. Time course for the oxidation of **1a** with O_2 catalyzed by fresh and recovered Mg_6MnO_8-MA. Reaction conditions: catalyst (0.1 g), **1a** (0.5 mmol), *n*-octane (2 mL), pO_2 (1 atm), 50 °C.

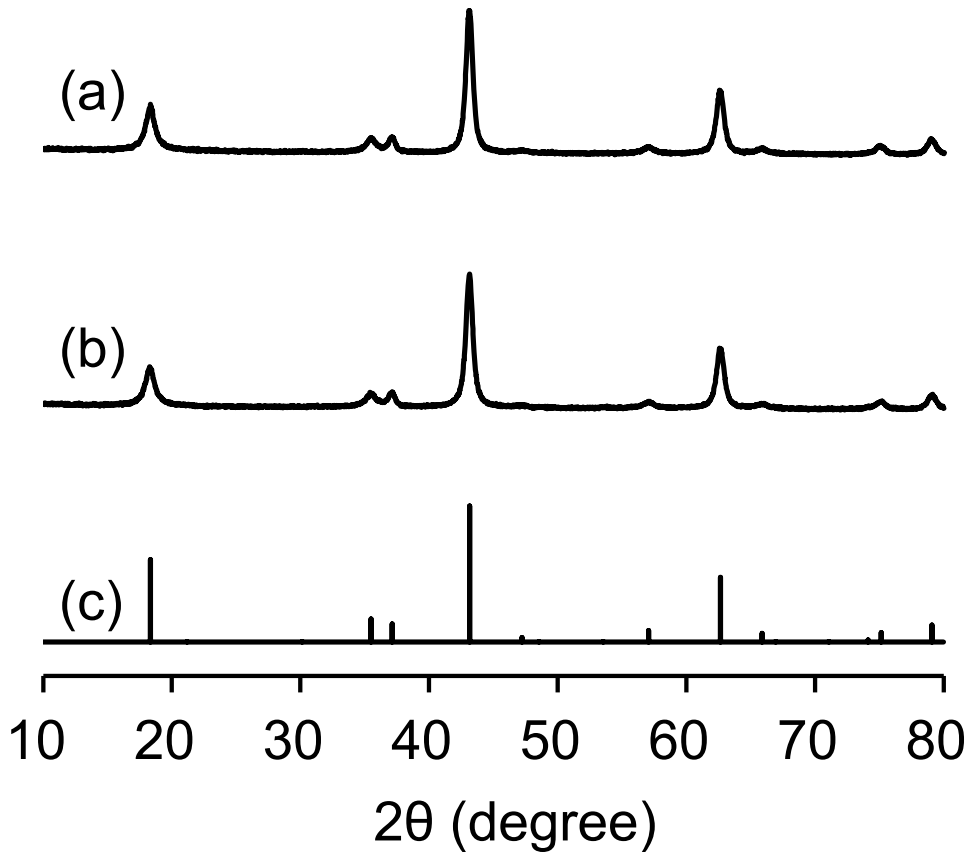

Figure S3. XRD patterns for (a) fresh Mg_6MnO_8-MA, (b) recovered Mg_6MnO_8-MA after the catalytic oxidation of **1a**, and (c) Mg_6MnO_8 (JCPDS 01-073-2156). The reaction conditions are the same as those in Figure 4b.

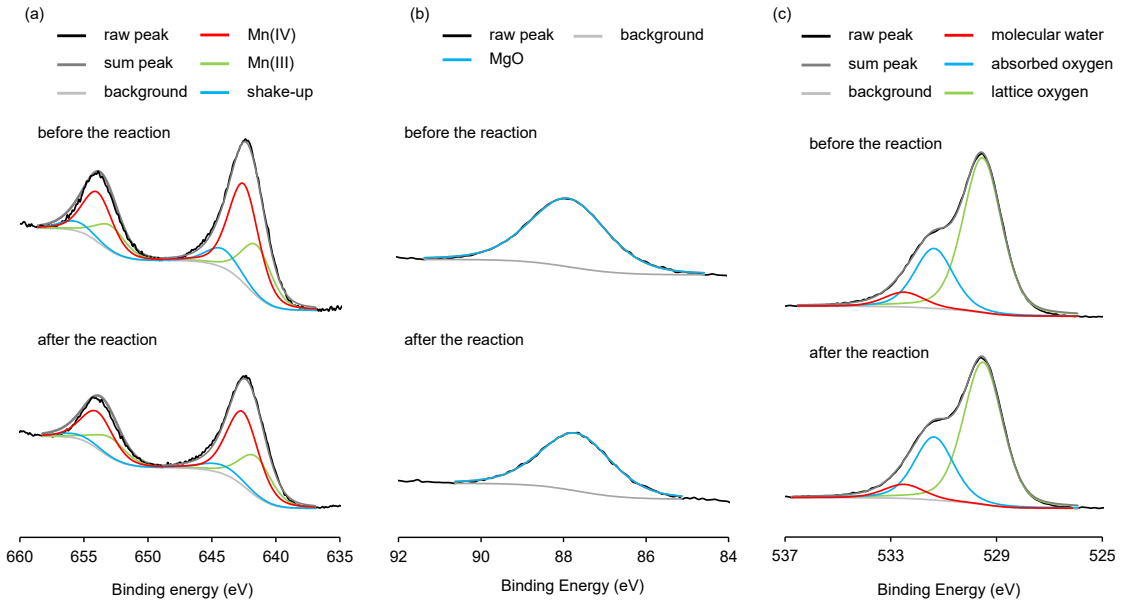

Figure S4. XPS (a) Mn 2p, (b) Mg 2s, (c) O 1s spectra of fresh Mg_6MnO_8-MA and recovered Mg_6MnO_8-MA after the catalytic oxidation of **1a**. The reaction conditions are the same as those in Figure 4b.

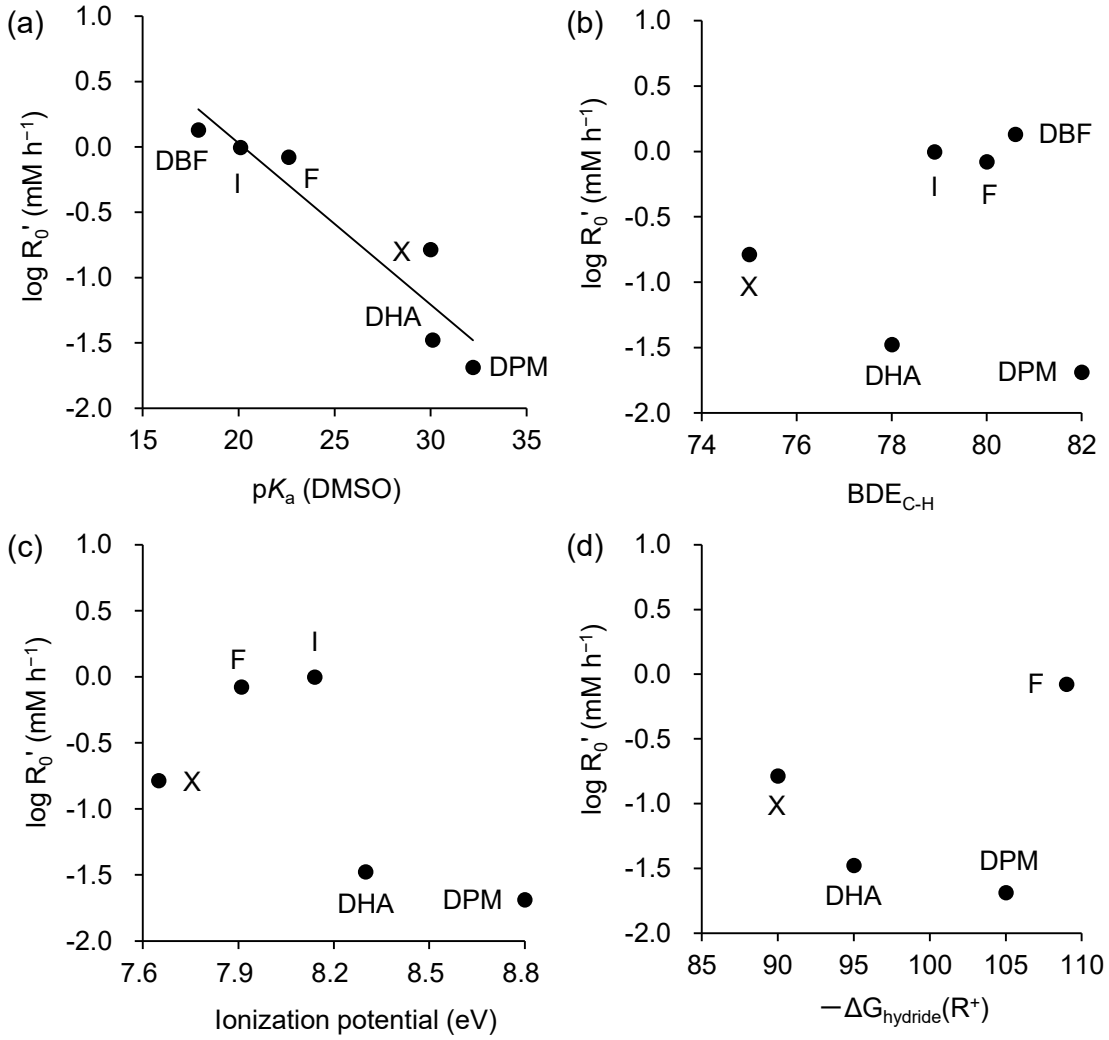

Figure S5. Log R_0' for the oxidations of alkylarenes (xanthene (X), 9,10-dihydroanthracene (DHA), indene (I), diphenylmethane (DPM), 2,7-Dibromo-9-fluorenone (DBF) and fluorene (F)) as a function of (a) pK_a, (b) homolytic bond dissociation energy (c) ionization potential, and (d) heterolytic bond dissociation energy. Reaction conditions were as follows: Alkylarene (0.3 mmol), Mg_6MnO_8 (30 mg), chlorobenzene (4 mL), 50 °C, pO_2 (1 atm). The initial rates (-d[substrate]/dt, R_0) were determined from the slopes of reaction profiles ([substrate]$_0$-[substrate]t vs. time plots) at low conversions (<20%) of the substrates. Data of pK_a are taken from references S57, S58, and S59. BDE is the free energy of R-H homolytic bond disassociation. Data of BDE are taken from refs. S57, S58, and S59. $-\Delta G_{hydride}(R^+)$ is the free energy of R-H heterolytic bond disassociation. Data of $-\Delta G_{hydride}(R^+)$ are from refs. S60 and S61. Date of ionization potential are from NIST at http://webbook.nist.gov/chemistry.